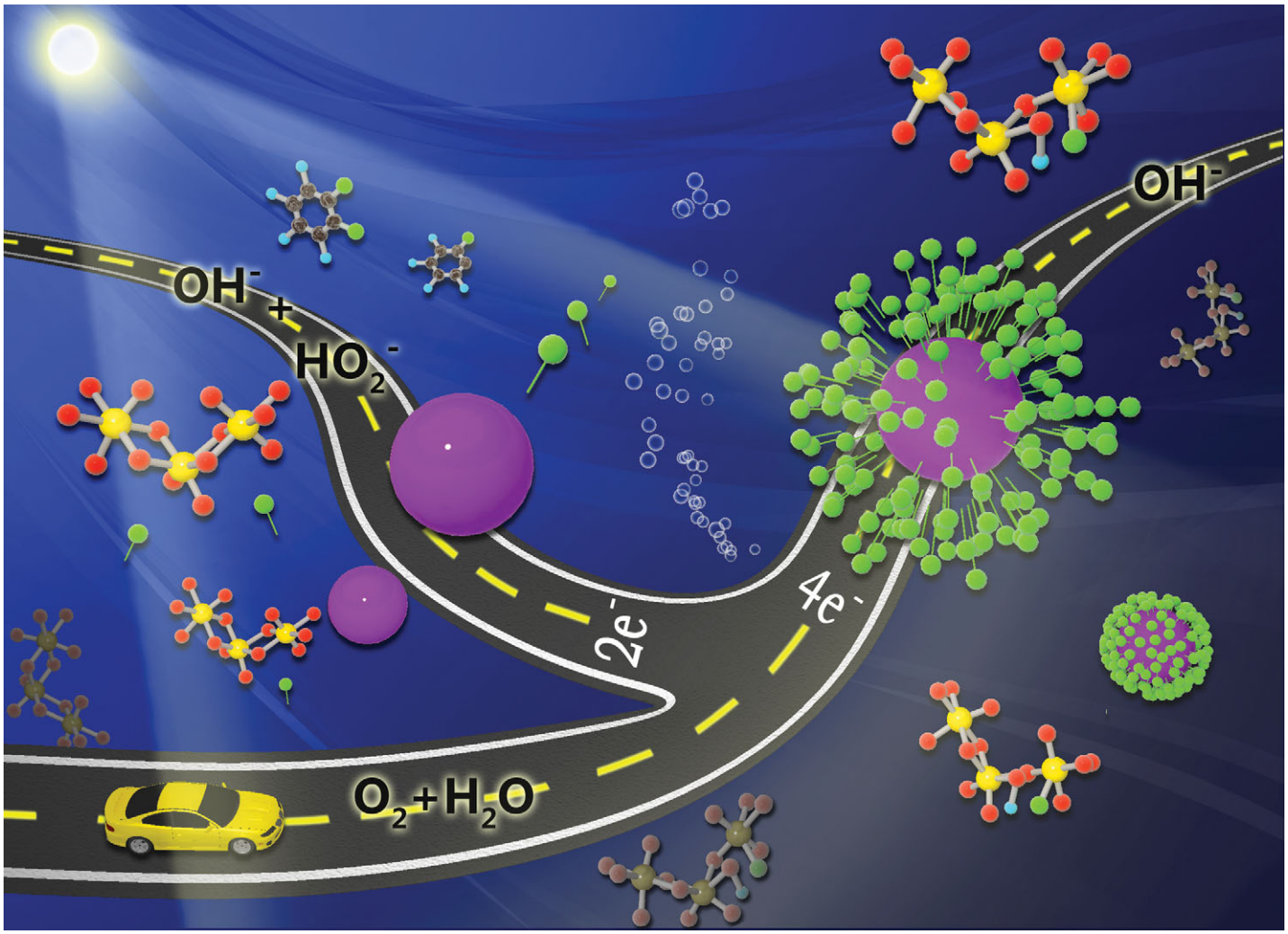

Showcasing work from the laboratory of Ligui Li and Shaowei Chen at the New Energy Research Institute, College of Environment and Energy, South China University of Technology, P. R. China.

Oxygen electroreduction promoted by quasi oxygen vacancies in metal oxide nanoparticles prepared by photoinduced chlorine doping

Quasi oxygen vacancies on ITO nanoparticles were facilely prepared by photoinduced chlorine doping to effectively promote oxygen electroreduction in an alkaline media, which may open new avenue for the development of oxygen-deficient metal oxides based electrocatalysts.

As featured in:

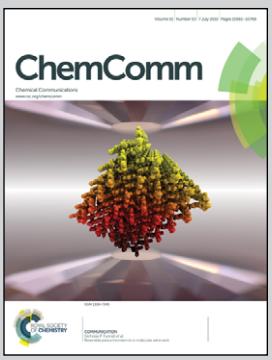

See Ligui Li, Shaowei Chen *et al.*, *Chem. Commun.*, 2015, **51**, 10620.

ROYAL SOCIETY OF CHEMISTRY

www.rsc.org/chemcomm

Registered charity number: 207890

ChemComm

COMMUNICATION

View Article Online
View Journal | View Issue

Cite this: *Chem. Commun.*, 2015, **51**, 10620

Received 4th April 2015,
Accepted 16th May 2015

DOI: 10.1039/c5cc02808f

www.rsc.org/chemcomm

Oxygen electroreduction promoted by quasi oxygen vacancies in metal oxide nanoparticles prepared by photoinduced chlorine doping†

Nan Wang,‡[a] Wenhan Niu,‡[a] Ligui Li,*[a] Ji Liu,[a] Zhenghua Tang,[a] Weijia Zhou[a] and Shaowei Chen*[ab]

Quasi oxygen-deficient indium tin oxide nanoparticles (ITO NPs) were prepared by photoinduced chlorine doping, and exhibited much enhanced electrocatalytic activity for oxygen reduction reaction (ORR) in alkaline media, as compared with pristine ITO.

Metal oxides[1] and their perovskites[2,3] have been attracting extensive research interest as emerging potential catalysts for ORR in alkaline fuel cells and rechargeable metal–air batteries, mainly because of their low costs, widespread availability, ease of preparation, appealing catalytic activity and high stability in the working potential range. Nevertheless, metal oxides are generally much less active than noble-metal catalysts, especially in terms of overpotential, diffusion limited current and the capability to catalyze four-electron reduction. It has been found that the ORR activity may be enhanced by oxygen vacancies on the oxide surface, which are generally formed by high-temperature calcination.[1,2] Yet this is incompatible with materials that are not stable at high temperatures. Therefore, it remains of high demand to explore novel, effective methods for the preparation of oxygen-deficient metal oxide catalysts under mild conditions from both industrial and academic points of view. This is the primary motivation of the present study.

ITO is a highly conductive semiconductor that exhibits relatively high stability in harsh environments and strong resistance to oxidation at high potentials, as compared with carbon-based materials such as porous carbons, graphene and carbon nanotubes.[4] Therefore, there is increasing interest in using ITO NPs as novel catalyst supports[5,6] or stabilizers[4] for metal catalysts. However, studies of the catalytic activity of ITO itself, in particular for ORR, have been scarce, to the best of our knowledge.

Herein, we carried out a systematic study of the ORR activity of ITO NPs and use them as an illustrating example to examine the effect of photoinduced chlorine doping, which led to the formation of quasi oxygen vacancies, on the corresponding ORR activity. The resulting nanoparticles showed rather remarkable ORR activity in alkaline media, a performance much higher than that of pristine ITO NPs.

Experimentally, ITO NPs were prepared according to a literature procedure[4] based on solvothermal treatment of indium acetylacetonate [In(acac)$_3$] and tin(IV) *tert*-butoxide [Sn(O*t*Bu)$_4$] in benzyl alcohol at controlled temperatures. Chlorine-doped ITO (Cl-ITO) NPs were then prepared by UV photoirradiation of the ITO NPs for 5 min in *o*-dichlorobenzene (ODCB),[7] as depicted in Scheme 1 (details in ESI†).

Fig. 1a shows a representative TEM image of the Cl-ITO nanoparticles. It can be seen that the nanoparticles were mostly spherical in shape with the diameters in the range of 5 to 10 nm. From high-resolution TEM measurements in Fig. 1b, one can see clearly-defined lattice fringes with a spacing of 0.29 nm, which is consistent with the *d*-spacing of the (222) crystalline planes of ITO, indicating the highly crystalline nature of the Cl-ITO NPs and the retention of the ITO crystalline structure after chlorine doping (Fig. S1, ESI†). Statistical analysis based on about two hundred nanoparticles shows that

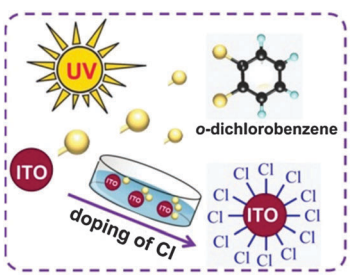

Scheme 1 Schematic of the preparation of Cl-ITO NPs.

[a] *New Energy Research Institute, College of Environment and Energy, South China University of Technology, Guangzhou Higher Education Mega Center, Guangzhou 510006, China. E-mail: esguili@scut.edu.cn*

[b] *Department of Chemistry and Biochemistry, University of California, 1156 High Street, Santa Cruz, California 95064, USA. E-mail: shaowei@ucsc.edu*

† Electronic supplementary information (ESI) available: Experimental procedures, and additional TEM, spectroscopic and voltammetric data. See DOI: 10.1039/c5cc02808f

‡ These authors contribute equally to this work.

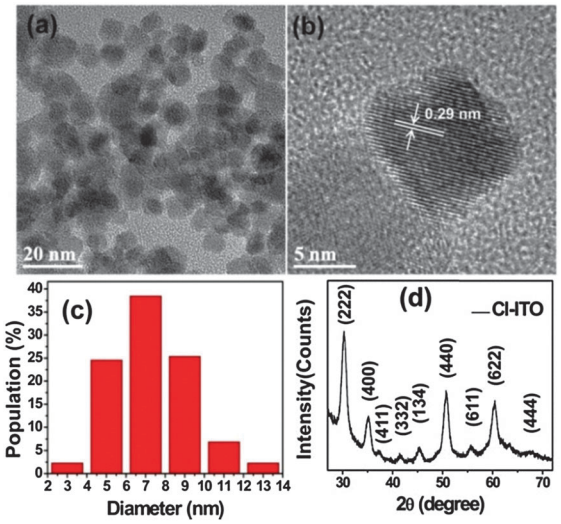

Fig. 1 (a) TEM and (b) HRTEM images of Cl-ITO NPs, with (c) the corresponding core size histogram and (d) XRD diffraction profile.

the average diameter of the Cl-ITO NPs is *ca.* 7.03 ± 0.51 nm, as manifested by the core size histogram in Fig. 1c. This is almost the same as that of the pristine ITO NPs (Fig. S1, ESI†). Consistent results were obtained in X-ray diffraction (XRD) studies, as depicted in Fig. 1d, where all the diffraction peaks can be indexed to the cubic bixbyite phase of In_2O_3 (PDF No. 6-416).[8] Note that no peaks can be assigned to SnO_2, indicating the formation of a solid solution rather than a mixture of indium oxide and tin oxide[4] in Cl-ITO. The size of the crystallites along the [222] direction was estimated to be 7.51 ± 0.23 nm by using the Scherrer equation, in good agreement with the TEM results in Fig. 1a.

X-ray photoelectron spectroscopy (XPS) measurements were then conducted to probe the elemental composition of the nanoparticles. In the survey spectrum of ITO nanoparticles (black curve, Fig. 2a), only the elements of In, Sn, and O can be identified. Consistent spectral features can be seen for the Cl-ITO samples (red curve). Importantly, the latter also exhibited two additional peaks at 284.10 eV and 199.06 eV (indicated by blue triangles), which may be assigned to the Cl 2s and 2p electrons, respectively, suggesting effective doping of Cl into the ITO nanoparticles. Note that these Cl signals were absent in the as-prepared ITO NPs or the ITO NPs that were immersed into ODCB but without UV photoirradiation (Fig. S2, ESI†), indicating

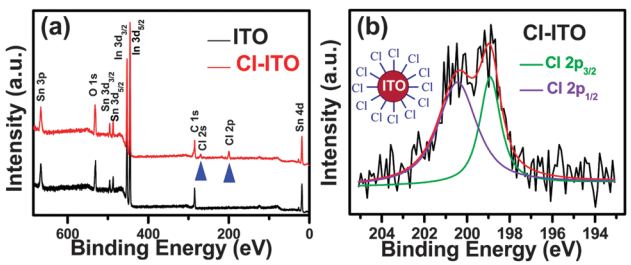

Fig. 2 (a) XPS survey spectra of Cl-ITO and (b) the high-resolution scan of Cl 2p electrons. Inset is the sketch of a Cl-ITO NP.

that Cl was actually chemically bonded to the ITO nanoparticle surface in Cl-ITO after UV treatment. Furthermore, high-resolution scan of the Cl 2p electrons in Cl-ITO (Fig. 2b) yielded only a doublet at 200.56 eV and 199.06 eV, consistent with the Cl $2p_{1/2}$ and Cl $2p_{3/2}$ electrons in $InCl_3$, respectively. This suggests a uniform bonding configuration of Cl in the sample. Similar behaviors have been observed previously.[7] In addition, based on the integrated peak areas, the loading of Cl dopants in Cl-ITO was estimated to be 3.9 at%. Because of this low concentration of Cl doping, the UV-vis absorption spectra of ITO and Cl-ITO NPs were virtually identical (Fig. S3, ESI†).

Interestingly, the Cl-ITO NPs exhibited apparent electrocatalytic activity for ORR (experimental details in ESI†). Cyclic voltammetric measurements were first carried out in N_2- and O_2-saturated 0.1 M KOH solutions at a mass loading of 102.0 μg cm^{-2} on a glassy carbon electrode. As depicted in Fig. 3a, in the N_2-saturated electrolyte solution (black dashed curves), both ITO and Cl-ITO exhibited largely a featureless double-layer charging profile. In contrast, when the solution was saturated with O_2 (red solid curves), two apparent cathode peaks emerged at +0.50 V and +0.19 V, suggesting the effective ORR activity of the oxide nanoparticles. More significantly, the peak currents of the Cl-ITO NPs (0.18 mA cm^{-2} at +0.50 V, 0.22 mA cm^{-2} at +0.19 V) were markedly higher than those of the pristine ITO (0.15 mA cm^{-2} at +0.50 V, 0.20 mA cm^{-2} at +0.19 V), signifying much enhanced ORR activity by Cl doping.

The ORR activity and kinetics were further examined by using rotating disk electrode (RDE) voltammetry in the same O_2-saturated 0.1 M KOH solution. From Fig. 3b, one can see that for both pristine ITO and Cl-ITO NPs, nonzero cathodic currents started to appear when the electrode potential was swept negatively beyond +0.67 V; yet, a much higher limiting current was observed with Cl-ITO. For instance, at 0 V, the limiting current density was only 2.05 mA cm^{-2} for ITO, but increased markedly to 2.64 mA cm^{-2} for Cl-ITO, again signifying enhanced ORR activity by surface Cl doping.

Fig. 3c depicts the RRDE voltammograms of the Cl-ITO NPs-modified electrode where the ring potential was set at +1.5 V (the data for pristine ITO NPs were included in Fig. S3, ESI†). One can see that the disk currents increased with increasing electrode rotation rate and the ring currents were about one-order of magnitude lower than those at the disk, suggesting rather effective reduction of oxygen catalyzed by the Cl-ITO NPs, as manifested by the number of electron transfer (n, eqn (1)) and the H_2O_2 yield (eqn (2)) involved in ORR,

$$n = \frac{4I_{\mathrm{Disk}}}{I_{\mathrm{Ring}}/N + I_{\mathrm{Disk}}} \quad (1)$$

$$\mathrm{H_2O_2}\% = \frac{200I_{\mathrm{Ring}}/N}{I_{\mathrm{Ring}}/N + I_{\mathrm{Disk}}} \quad (2)$$

where N is the collection efficiency (37%), I_{Disk} and I_{Ring} are the voltammetric currents at the disk and ring electrodes, respectively. From Fig. 3d (top), one can see that the n values for ITO were in the range of 2.3 to 2.8 at 0.3–0.0 V, but increased markedly to 2.9 to 3.4 with Cl-ITO. This observation indicates

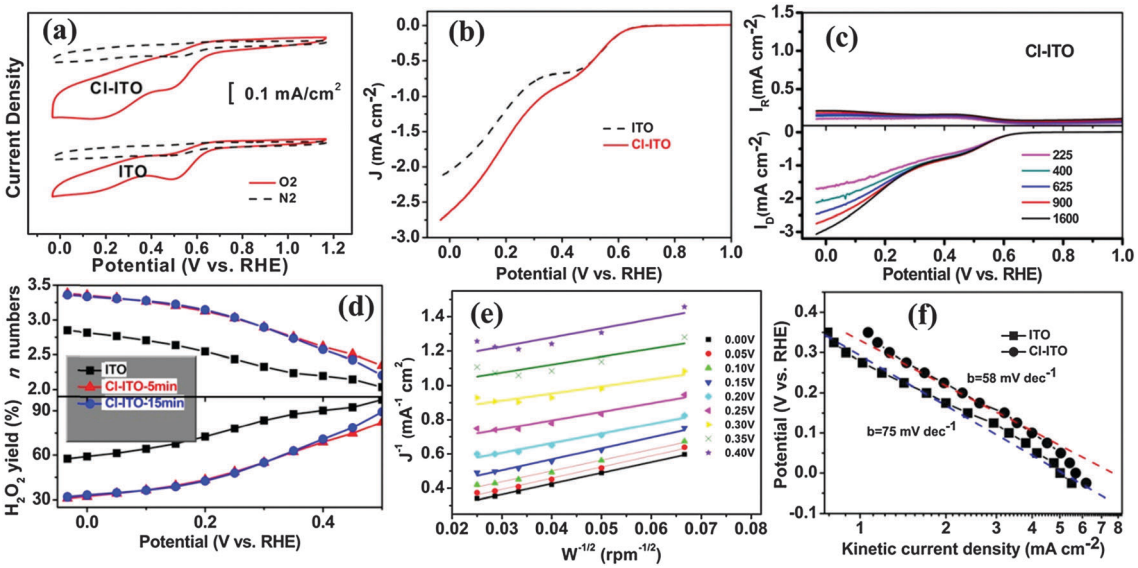

Fig. 3 (a) Cyclic and (b) RDE voltammograms of ITO and Cl-ITO at an electrode rotation rate of 900 rpm, (c) RRDE of Cl-ITO at different rotation rates (specified in figure legends); (d) plots of number of electron transfer and H_2O_2 yield at ITO and Cl-ITO. (e) K–L plots of Cl-ITO, and (f) Tafel plots at ITO and Cl-ITO. Measurements were all conducted on a glassy carbon electrode at a catalyst loading of 102.0 μg cm^{-2} in O_2-saturated 0.1 M KOH at a potential sweep rate of 10 mV s^{-1}.

that ORR on Cl-ITO mostly proceeded *via* the 4-electron reduction route (fully reduced to OH^-) while on ITO it followed predominantly a 2-electron process with peroxides as the predominant final products. In fact, the percent yield of H_2O_2 decreased by about 30% with Cl-ITO as compared to that of ITO (Fig. 3d, bottom). This suggests that Cl doping indeed served as an effective method for the enhancement of the ORR activity of ITO.

Note that extending the UV irradiation time to, for example 15 min, led to virtually no change of the *n* values or H_2O_2% yield (Fig. 3d), indicating that a 5 min exposure time for Cl doping was enough to produce the best Cl-ITO electrocatalyst within the present experimental context.

The corresponding Koutecky–Levich (K–L) plots were depicted in Fig. 3e which exhibit good linearity and parallelism over the potential range from 0.00 to +0.40 V, suggesting the first-order reaction kinetics of ORR with respect to oxygen concentration in the solution. Similar behaviors were observed with the pristine ITO as well (Fig. S4, ESI†). The corresponding Tafel plots were depicted in Fig. 3f, where one can see that the slopes of Cl-ITO (58 mV dec^{-1}) and ITO (75 mV dec^{-1}) were rather close, indicating a similar reaction mechanism with the rate-determining step being the first electron reduction of oxygen. Yet, Cl-ITO exhibited a markedly higher current density than ITO. For instance, at +0.25 V, the kinetic current density was 1.68 mA cm^{-2} with Cl-ITO but only 1.19 mA cm^{-2} with ITO, signifying that chlorine doping indeed enhanced the ORR activity.

Experimentally a gradual loss of Cl dopants was observed. For instance, after 100 cycles within the potential range of −0.03 to +1.12 V at the potential sweep rate of 10 mV s^{-1}, the concentration of Cl dopants was found to decrease to 2.0 at% (Fig. S5, ESI†). However, chronoamperometric measurements (Fig. S6, ESI†) showed that during more than 8 h's continuous operation, the ORR performance of Cl-ITO NPs remained superior to that of pristine ITO NPs.

Although the mechanism is not yet fully understood, it is likely that the enhanced ORR activity of Cl-ITO, as compared with that of pristine ITO, may be attributed to Cl doping that led to the formation of surface defects with variable oxygen stoichiometry. As shown in Scheme 2, in the crystalline lattice of In_2O_3, each In atom coordinates with six O atoms, and each O atom with two In atoms. The substitution of one O atom (electronegativity 3.44) by Cl (electronegativity 3.16) decreases the local O : In stoichiometric ratio, leading to the formation of quasi oxygen-deficient sites that were advantageous for oxygen binding,[1,2,9] a critical first step in ORR. Further research is desired to unravel the mechanism of ORR on Cl-ITO.

Note that whereas the performance of Cl-ITO remains subpar as compared to that of state-of-the art Pt/C catalysts,[10,11] the fact that Cl-modification of ITO surfaces markedly improved the ORR activity suggests that the electrocatalytic performance might be further enhanced by deliberate engineering of the ITO nanoparticle surfaces with other dopants.

In summary, Cl-ITO NPs were successfully prepared by UV photo irradiation of ITO NPs in the presence of ODCB.

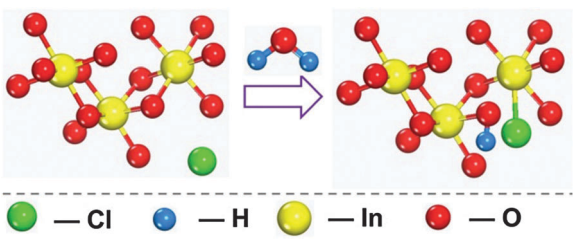

Scheme 2 Formation of local quasi-oxygen vacancy due to the substitution of O by Cl at the In atom in the right.

Electrochemical measurements showed that the electrocatalytic activity of Cl-ITO in ORR was substantially enhanced as compared with that of pristine ITO, within the context of diffusion limiting current and the number of electron transfer processes involved in ORR. This was likely due to the formation of quasi oxygen-deficient sites on Cl-ITO surfaces that were advantageous for oxygen binding. Results from the present work suggest a novel and facile method for the improvement of the ORR activity of metal oxides.

This work was supported by the National Recruitment Program of Global Experts. L.G.L. acknowledges support from the National Natural Science Foundation of China (NSFC 51402111) and the Fundamental Research Funds for the Central Universities (SCUT Grant No. 2013ZM0019). S.W.C. thanks the National Science Foundation (CHE-1265635 and DMR-1409396) for partial support of the work.

Notes and references

1 F. Cheng, T. Zhang, Y. Zhang, J. Du, X. Han and J. Chen, *Angew. Chem., Int. Ed.*, 2013, **52**, 2474.
2 J. Kim, X. Yin, K.-C. Tsao, S. Fang and H. Yang, *J. Am. Chem. Soc.*, 2014, **136**, 14646.
3 J. Suntivich, H. A. Gasteiger, N. Yabuuchi, H. Nakanishi, J. B. Goodenough and Y. Shao-Horn, *Nat. Chem.*, 2011, **3**, 546.
4 R. Kou, Y. Shao, D. Mei, Z. Nie, D. Wang, C. Wang, V. V. Viswanathan, S. Park, I. A. Aksay, Y. Lin, Y. Wang and J. Liu, *J. Am. Chem. Soc.*, 2011, **133**, 2541–2547.
5 G. Chang, M. Oyama and K. Hirao, *J. Phys. Chem. B*, 2006, **110**, 1860.
6 Y. Song, Y. Ma, Y. Wang, J. Di and Y. Tu, *Electrochim. Acta*, 2010, **55**, 4909.
7 M. G. Helander, Z. B. Wang, J. Qiu, M. T. Greiner, D. P. Puzzo, Z. W. Liu and Z. H. Lu, *Science*, 2011, **332**, 944.
8 Y. Hao, G. Meng, C. Ye and L. Zhang, *Cryst. Growth Des.*, 2005, **5**, 1617.
9 X. Han, Y. Hu, J. Yang, F. Cheng and J. Chen, *Chem. Commun.*, 2014, **50**, 1497.
10 Y. Song and S. W. Chen, *ACS Appl. Mater. Interfaces*, 2014, **6**, 14050–14060.
11 G. Q. He, Y. Song, K. Liu, A. Walter, S. Chen and S. W. Chen, *ACS Catal.*, 2013, **3**, 831–838.